

PG 1553+113: FIVE YEARS OF OBSERVATIONS WITH MAGIC

J. ALEKSIĆ¹, E. A. ALVAREZ², L. A. ANTONELLI³, P. ANTORANZ⁴, M. ASENSIO², M. BACKES⁵, J. A. BARRIO², D. BASTIERI⁶, J. BECERRA GONZÁLEZ^{7,8}, W. BEDNAREK⁹, A. BERDYUGIN¹⁰, K. BERGER^{7,8}, E. BERNARDINI¹¹, A. BILAND¹², O. BLANCH¹, R. K. BOCK¹³, A. BOLLER¹², G. BONNOLI³, D. BORLA TRIDON¹³, I. BRAUN¹², T. BRETZ^{14,31}, A. CAÑELLAS¹⁵, E. CARMONA¹³, A. CAROSI³, P. COLIN¹³, E. COLOMBO⁷, J. L. CONTRERAS², J. CORTINA¹, L. COSSIO¹⁶, S. COVINO³, F. DAZZI^{16,32}, A. DE ANGELIS¹⁶, G. DE CANEVA¹¹, E. DE CEA DEL POZO¹⁷, B. DE LOTTO¹⁶, C. DELGADO MENDEZ^{7,33}, A. DIAGO ORTEGA^{7,8}, M. DOERT⁵, A. DOMÍNGUEZ¹⁸, D. DOMINIS PRESTER¹⁹, D. DORNER¹², M. DORO²⁰, D. ELSAESSER¹⁴, D. FERENC¹⁹, M. V. FONSECA², L. FONT²⁰, C. FRUCK¹³, R. J. GARCÍA LÓPEZ^{7,8}, M. GARCZARCZYK⁷, D. GARRIDO²⁰, G. GIAVITTO¹, N. GODINOVIC¹⁹, D. HADASCH¹⁷, D. HÄFNER¹³, A. HERRERO^{7,8}, D. HILDEBRAND¹², D. HÖHNE-MÖNCH¹⁴, J. HOSE¹³, D. HRUPEC¹⁹, B. HUBER¹², T. JOGLER¹³, H. KELLERMANN¹³, S. KLEPNER¹, T. KRÄHENBÜHL¹², J. KRAUSE¹³, A. LA BARBERA³, D. LELAS¹⁹, E. LEONARDO⁴, E. LINDFORS¹⁰, S. LOMBARDI⁶, M. LÓPEZ², A. LÓPEZ-ORAMAS¹, E. LORENZ^{12,13}, M. MAKARIEV²¹, G. MANEVA²¹, N. MANKUZHIYIL¹⁶, K. MANNHEIM¹⁴, L. MARASCHI³, M. MARIOTTI⁶, M. MARTÍNEZ¹, D. MAZIN^{1,13}, M. MEUCCI⁴, J. M. MIRANDA⁴, R. MIRZOYAN¹³, H. MIYAMOTO¹³, J. MOLDÓN¹⁵, A. MORALEJO¹, P. MUNAR-ADROVER¹⁵, D. NIETO², K. NILSSON^{10,34}, R. ORITO¹³, I. OYA², D. PANEQUE¹³, R. PAOLETTI⁴, S. PARDO², J. M. PAREDES¹⁵, S. PARTINI⁴, M. PASANEN¹⁰, F. PAUSS¹², M. A. PEREZ-TORRES¹, M. PERSIC^{16,22}, L. PERUZZO⁶, M. PILIA²³, J. POCHON⁷, F. PRADA¹⁸, P. G. PRADA MORONI²⁴, E. PRANDINI⁶, I. PULJAK¹⁹, I. REICHARDT¹, R. REINTHAL¹⁰, W. RHODE⁵, M. RIBÓ¹⁵, J. RICO^{1,25}, S. RÜGAMER¹⁴, A. SAGGION⁶, K. SAITO¹³, T. Y. SAITO¹³, M. SALVATI³, K. SATALECKA², V. SCALZOTTO⁶, V. SCAPIN², C. SCHULTZ⁶, T. SCHWEIZER¹³, M. SHAYDUK¹³, S. N. SHORE²⁴, A. SILLANPÄÄ¹⁰, J. SITAREK⁹, D. SOBCZYNSKA⁹, F. SPANIER¹⁴, S. SPIRO³, V. STAMATESCU¹, A. STAMERRA⁴, B. STEINKE¹³, J. STORZ¹⁴, N. STRAH⁵, T. SURIC¹⁹, L. TAKALO¹⁰, H. TAKAMI¹³, F. TAVECCHIO³, P. TEMNIKOV²¹, T. TERZIC¹⁹, D. TESCARO²⁴, M. TESHIMA¹³, O. TIBOLLA¹⁴, D. F. TORRES^{17,25}, A. TREVES²³, M.UELLENBECK⁵, H. VANKOV²¹, P. VOGLER¹², R. M. WAGNER¹³, Q. WEITZEL¹², V. ZABALZA¹⁵, F. ZANDANEL¹⁸, R. ZANIN¹, S. BUSON⁶, D. HORAN²⁶, S. LARSSON^{27,28,29}, AND F. D'AMMANDO³⁰

¹ IFAE, Edifici Cn., Campus UAB, E-08193 Bellaterra, Spain

² Grupo de Física Atlas Energías, Universidad Complutense, E-28040 Madrid, Spain

³ INAF National Institute for Astrophysics, I-00136 Rome, Italy; fabrizio.tavecchio@brera.inaf.it

⁴ Dipartimento di Fisica, Università di Siena and INFN Pisa, I-53100 Siena, Italy

⁵ Fakultät für Physik, Technische Universität Dortmund, D-44221 Dortmund, Germany

⁶ Dipartimento di Fisica, Università di Padova and INFN, I-35131 Padova, Italy; elisa.prandini@pd.infn.it

⁷ Inst. de Astrofísica de Canarias, E-38200 La Laguna, Tenerife, Spain

⁸ Depto. de Astrofísica, Universidad de La Laguna, E-38206 La Laguna, Spain

⁹ Department of Astrophysics, University of Łódź, PL-90236 Lodz, Poland

¹⁰ Tuorla Observatory, University of Turku, FI-21500 Piikkiö, Finland

¹¹ Deutsches Elektronen-Synchrotron (DESY), D-15738 Zeuthen, Germany

¹² ETH Zurich, CH-8093, Wolfgang-Pauli-Str. 15, CH-8093 Zürich-Hönggberg, Switzerland

¹³ Max-Planck-Institut für Physik, D-80805 München, Germany

¹⁴ Fakultät für Physik und Astronomie, Universität Würzburg, D-97074 Würzburg, Germany

¹⁵ Facultat de Física, Universitat de Barcelona (ICC/IEEC), E-08028 Barcelona, Spain

¹⁶ Dipartimento di Fisica Sperimentale, Università di Udine and INFN Trieste, I-33100 Udine, Italy

¹⁷ Institut de Ciències de l'Espai (IEEC-CSIC), E-08193 Bellaterra, Spain

¹⁸ Inst. de Astrofísica de Andalucía (CSIC), E-18080 Granada, Spain

¹⁹ Croatian MAGIC Consortium, Rudjer Boskovic Institute, University of Rijeka and University of Split, HR-10000 Zagreb, Croatia

²⁰ Facultat de Física, Universitat Autònoma de Barcelona, E-08193 Bellaterra, Spain

²¹ Inst. for Nucl. Research and Nucl. Energy, BG-1784 Sofia, Bulgaria

²² INAF/Osservatorio Astronomico and INFN, I-34143 Trieste, Italy

²³ Dipartimento di Fisica e Matematica, Università dell'Insubria, Como, I-22100 Como, Italy

²⁴ Dipartimento di Fisica, Università di Pisa and INFN Pisa, Largo B. Pontecorvo, 3-I-56127 Pisa, Italy

²⁵ Institució Catalana de Recerca i Estudis Avançats (ICREA), E-08010 Barcelona, Spain

²⁶ Laboratoire Leprince-Ringuet, Ecole polytechnique, CNRS/IN2P3, Palaiseau, France

²⁷ Department of Physics, Stockholm University, AlbaNova, SE-106 91 Stockholm, Sweden

²⁸ The Oskar Klein Center for Cosmoparticle Physics, AlbaNova, SE-106 91 Stockholm, Sweden

²⁹ Department of Astronomy, Stockholm University, SE-106 91 Stockholm, Sweden

³⁰ Consorzio Interuniversitario Fisica Spaziale (CIFS), v.le Settimio Severo 63, I-10133 Torino, Italy

Received 2011 July 1; accepted 2012 January 7; published 2012 March 5

ABSTRACT

We present the results of five years (2005–2009) of MAGIC observations of the BL Lac object PG 1553+113 at very high energies (VHEs; $E > 100$ GeV). Power-law fits of the individual years are compatible with a steady mean photon index $\Gamma = 4.27 \pm 0.14$. In the last three years of data, the flux level above 150 GeV shows a clear variability (probability of constant flux $< 0.001\%$). The flux variations are modest, lying in the range from 4% to 11% of the Crab Nebula flux. Simultaneous optical data also show only modest variability that seems to be correlated with VHE gamma-ray variability. We also performed a temporal analysis of (all available) simultaneous *Fermi*/Large Area Telescope data of PG 1553+113 above 1 GeV, which reveals hints of variability in the 2008–2009 sample. Finally, we present a combination of the mean spectrum measured at VHEs with archival data available for other

wavelengths. The mean spectral energy distribution can be modeled with a one-zone synchrotron self-Compton model, which gives the main physical parameters governing the VHE emission in the blazar jet.

Key words: BL Lacertae objects: individual (PG 1553+113) – gamma rays: galaxies – radiation mechanisms: non-thermal

Online-only material: color figures

1. INTRODUCTION

The majority of extragalactic γ -ray sources, both at GeV energies and above 100 GeV, are blazars, radio-loud active galactic nuclei with a relativistic jet pointing toward the Earth. Their emission is dominated by the non-thermal continuum produced within the jet and boosted by relativistic effects (Urry & Padovani 1995). The spectral energy distribution (SED) displays two broad peaks, widely interpreted as due to synchrotron, a low-frequency peak, and inverse Compton, a high-frequency peak, mechanism (although the high-energy peak could also be the result of hadronic processes, as proposed in Mannheim 1993). Among blazars, BL Lac objects are characterized by extremely weak emission lines in their optical spectra, which often makes measuring of their redshifts difficult. The large majority of extragalactic sources detected above 100 GeV are BL Lac objects, in which the peak of the synchrotron bump is located in the UV–X-ray bands and the high-energy peak around 100 GeV (these sources are often called high-frequency-peaked BL Lac objects (HBLs)). PG 1553+113 is a BL Lac object discovered by Green et al. (1986). The large X-ray to radio flux ratio makes this source a typical HBL. Indeed, its synchrotron peak is located between the UV and X-ray bands. Its optical spectrum is featureless, preventing the direct determination of the redshift. Indirect methods based on the non detection of the characteristic lines and of the host galaxy provide lower limits, ranging from 0.09 to 0.78 (Sbarufatti et al. 2006, 2005). The most recent estimate, based on the Ly α forest method, gives a $z \sim 0.40$ –0.45 (Danforth et al. 2010).

PG 1553+113 has been discovered as a very high energy (VHE) γ -ray emitter by H.E.S.S. (Aharonian et al. 2006a) and MAGIC (Albert et al. 2007a), with a flux of approximately 2% of that of the Crab Nebula above 200 GeV. The spectrum appears extremely soft (photon index $\Gamma \sim 4$), as expected by the absorption of VHE photons through interaction with the extragalactic background light (EBL) if the source is located at a relatively large redshift (Stecker et al. 1992). The absorption process, in fact, is a function of the energy of the photon and of the distance it has traveled. Spectra with indices $\Gamma \sim 4$ have been observed in blazars located at redshifts above 0.2.

VHE γ -ray observations have been used as an alternative method to constrain the distance of blazars. Aharonian et al. (2006b) proposed a way to set an upper limit on the distance of blazars based on the assumption that the VHE intrinsic spectrum, obtained by correcting the observed spectrum for the EBL absorption, cannot be harder than a fixed value given

by theory. The technique, applied to PG 1553+113, leads to an upper limit of $z < 0.74$. Recently, Prandini et al. (2010) extended this method using the spectrum measured at lower energies as limiting slope for the original spectrum, obtaining $z < 0.66$ for PG 1553+113, at 2σ level. Other approaches require the absence of a pile-up at high energies. With this method, Mazin & Goebel (2007) get $z < 0.42$. Hence, in the case of PG 1553+113, the upper limits obtained with these methods are in the range of the limits set by optical measurements. In this work, we adopt the redshift $z = 0.40$. Such a large redshift is also supported by the absence of significant points at energies above 700 GeV in the spectrum of the source.

At MeV–GeV energies, PG 1553+113 was not detected by EGRET, but it is well visible by the Large Area Telescope (LAT) on board *Fermi*, being detected with a significance above 10σ already in the first three months of observations (Abdo et al. 2009). Abdo et al. (2010b) show that the *Fermi*/LAT spectrum is surprisingly constant both in normalization and slope over ~ 200 days. Interestingly, a stability of the spectrum was also suggested by the H.E.S.S. and MAGIC observations, showing rather marginal variability during the 2005 and 2006 observations. The stability of the VHE γ -ray emission is in contrast to the behavior commonly observed in other TeV emitting BL Lac objects, showing rather pronounced variations at all timescales.

After its discovery, PG 1553+113 was regularly observed by MAGIC. In this paper, we present the analysis of the new data taken from 2007 to 2009, combined with previous observations. The differential and integral fluxes are analyzed, in comparison with partially simultaneous measurements at other wavelengths, and the stability of the spectrum over this long period is studied. Finally, we combine all the data available and model the SED with a one-zone synchrotron self-Compton (SSC) model, constraining the main physical parameters that govern the VHE emission in the blazar jet.

2. MAGIC OBSERVATIONS AND DATA ANALYSIS

Since autumn 2009, MAGIC (Cortina et al. 2009) is a stereo system composed by two Imaging Atmospheric Cherenkov Telescopes (IACTs) located on La Palma, Canary Islands, Spain (28.75°N, 17.89°W, 2240 m asl). In this paper, we present only data collected before the stereo upgrade, with a single telescope, MAGIC I (Baixeras et al. 2004), hereafter called MAGIC. The parabolic-shaped reflector, with a total mirror area of 236 m², allows MAGIC to collect the Cherenkov light and focus it into a multi-pixel camera, composed of 577 photo-multipliers. The MAGIC camera and trigger are designed to record data not only during dark nights, but also under moderate light conditions (i.e., moderate moon, twilight). Due to its comparatively low-trigger energy threshold of ~ 50 GeV, MAGIC is well suited to perform multiwavelength observations together with instruments operating in the GeV range.

The total field of view (FoV) of the MAGIC camera is 3°:5, and the effective collection area is of the order of 10⁵ m²

³¹ Now at Ecole polytechnique fédérale de Lausanne (EPFL), Lausanne, Switzerland.

³² Supported by INFN Padova.

³³ Now at Centro de Investigaciones Energéticas, Medioambientales y Tecnológicas (CIEMAT), Madrid, Spain.

³⁴ Now at Finnish Centre for Astronomy with ESO (FINCA), University of Turku, Finland.

Table 1
PG 1553+113 Final Data Set

Cycle	Date	Effective Time (min)	Zd (deg)	Rate (Hz)	DC (μ A)
III	2007 Mar 23	58	19–29	164	Dark night
	2007 Apr 19	32	22–28	155	Dark night
	2007 Apr 20	150	17–29	163	Dark night
	2007 Apr 21	115	17–24	155	Dark night
	2007 Apr 22	101	17–23	162	Dark night
	2007 Apr 23	143	17–27	161	Dark night
	2007 Apr 24	92	17–23	160	Dark night
	2008 Mar 17	58	17–19	150	Dark night
IV	2008 Mar 18	26	18–19	150	Dark night
	2008 Apr 1	43	20–26	167	Dark night
	2008 Apr 5	109	17–31	167	Dark night
	2008 Apr 13	97	17–22	147	Dark night
	2008 Apr 29	44	27–36	151	Dark night
	2008 May 3	24	26–31	146	Dark night
	2008 May 4	40	28–36	155	Dark night
	2008 May 5	38	26–33	150	Dark night
	2008 May 7	40	28–36	153	Dark night
	V	2009 Apr 16	93	17–27	133
2009 Apr 17		103	17–28	151	1.6–2.4
2009 Apr 18		126	17–28	168	0.7–1.7
2009 Apr 20		73	19–35	171	0.9–1.4
2009 Apr 21		57	23–34	177	0.8–1.0
2009 Jun 15		57	24–35	125	0.8–2.1

Notes. PG 1553+113 data set from 2007 to 2009 used in this study. From left to right: MAGIC Cycle of observation, first column, and corresponding dates in dd/mm/yy, second column; effective time of observation in minutes and zenith angle range in degrees, third and fourth columns. In the last two columns, the rate of the events after the image cleaning, in Hz, and the mean DC current in the camera, in unit of μ A, are shown. The night is considered as dark night, if the DC current while observing an extragalactic object is less than indicatively 1.2 μ A.

at 200 GeV for a source close to zenith. The incident light pulses are converted into analog signals, transmitted via optical fibers and digitized by 2 GHz fast analog to digital converters (FADCs).

PG 1553+113 was observed with the MAGIC telescope for nearly 19 hr in 2005 and 2006 (Albert et al. 2007a); it was also the subject of a multiwavelength campaign carried out in 2006 July with optical, X-ray, and TeV γ -ray telescopes (Albert et al. 2009). Here, we present the results of follow-up observations, performed for 14 hr in 2007 March–April, for nearly 26 hr in 2008 March–May, some of those simultaneously with other instruments (Aleksić et al. 2010), and for about 24 hr in 2009 March–July, which were partly taken in moderate light conditions (moon light). Unfortunately, both the 2008 and 2009 observations were severely affected by bad weather (including *calima*, i.e., Saharan sand dust in the atmosphere) that limited the final data set and resulted in an increased energy threshold.

All data analyzed here were taken in the false-source tracking (wobble) mode (Fomin et al. 1994), in which the telescope pointing was alternated every 20 minutes between two sky positions at 0.4 offset from the source. The zenith angle of 2007 observations varied from 17° to 30°, in 2008 it extended up to 36°, while in 2009 it covered the range from 17° to 35°.

The data were analyzed using the standard MAGIC analysis chain (Albert et al. 2008a; Aliu et al. 2009). Severe quality cuts based on event rate after night sky background suppression were applied to the sample; 28.7 hr of good quality data remained after these cuts, out of which 11.5 hr were taken in 2007, 8.7 hr

Table 2
PG 1553+113 Signal

Year	Time (hr)	Optical PSF (mm)	Energy Threshold (GeV)	Excesses	Significance (σ)
2007	11.5	13	80	1400 \pm 242	5.8
2008	8.7	13	150	542 \pm 69	8.1
2009	8.5	14.8	160	212 \pm 52	4.2

Notes. PG 1553+113 signal study. From left to right: year of observation, effective time of good quality data used for the signal analysis, optical point spread function (PSF), energy threshold of the analysis, number of excess events observed, and significance of the signal.

in 2008, and 8.5 hr in 2009. More details about the final data set can be found in Table 1. For the signal study, a cut in the parameter *size* removed events with a total charge less than 80 photoelectrons (phe) in the 2007 data set, and 200 phe in 2008 and 2009 data sets. In the latter case, this cut reduces the effect of the moon light.

Finally, for the spectrum determination an additional cut in PMT DC current, namely, above 2.5 μ A, was applied to the 2009 sample in order to reduce systematics due to the moon light (Britzger et al. 2009), resulting in 6.9 hr of good quality data. For the conclusive steps of the analysis, Monte Carlo (MC) simulations of γ -like events were used. Hadronic background suppression was achieved using the Random Forest (RF) method (Albert et al. 2008c), in which each event is assigned an additional parameter, the *hadronness*, which is related to the probability that the event is not γ -like. The RF method was also used in the energy estimation. The threshold of the analysis was estimated to be 80 GeV in 2007, 150 GeV in 2008, and 160 GeV in 2009, as shown in Table 2.

Due to changes in the telescope performance, the *sigma* of the optical point-spread function (PSF) of 2007 and 2008 was measured to be 13.0 mm, while in 2009 it was 14.8 mm. To take all these differences into account, the data were analyzed separately, using dedicated sets of simulated data.

3. VHE γ -RAY RESULTS

The 28.7 hr of good quality observations of PG 1553+113 carried out between 2007 and 2009 resulted in a signal of 8.8 σ of significance according to Equation (17) of Li & Ma (1983), obtained by combining the results from each year, listed in Table 2. The signal was extracted by analyzing the distribution of the parameter *alpha*, related to the incoming direction of the primary cosmic ray inducing the atmospheric shower. More details on the signal extraction with the *alpha* technique can be found in Albert et al. (2008b). For the signal detection, no cut in energy was applied.

The significance of the signal was 5.8 σ in 2007, 8.1 σ in 2008, and 4.2 σ in 2009. Due to a large difference in the energy thresholds and changes in the experimental conditions, the obtained fluxes cannot be compared directly. A detailed spectral analysis is necessary in order to study the source emission.

3.1. Integral Flux

In order to explore the VHE γ -ray emission of PG 1553+113 from each year, we compared the integral flux above 150 GeV. This value is a safe compromise taking into account the different energy thresholds. The final samples and the results of the spectral analyses are shown in Table 3.

Table 3
PG 1553+113 Measured Spectra

Year	$F > 150 \text{ GeV}$ ($\text{cm}^{-2} \text{ s}^{-1}$)	$F > 150 \text{ GeV}$ (Crab %)	f_0 ($\text{cm}^{-2} \text{ s}^{-1} \text{ TeV}^{-1}$)	Γ
2007	$(1.40 \pm 0.38) \times 10^{-11}$	4%	$(1.1 \pm 0.3) \times 10^{-10}$	4.1 ± 0.3
2008	$(3.70 \pm 0.47) \times 10^{-11}$	11%	$(2.6 \pm 0.3) \times 10^{-10}$	4.3 ± 0.4
2009	$(1.63 \pm 0.45) \times 10^{-11}$	5%	$(1.3 \pm 0.2) \times 10^{-10}$	3.6 ± 0.5

Notes. Spectra of the individual years of observations of PG 1553+113. From left to right: year of MAGIC observations, integral flux above 150 GeV in units of $\text{cm}^{-2} \text{ s}^{-1}$ and Crab Nebula %, normalization factor f_0 in units of $\text{cm}^{-2} \text{ s}^{-1} \text{ TeV}^{-1}$, and in the last column, the Γ index obtained by fitting the observed differential spectrum with a power law. The errors reported are statistical only. The systematic uncertainty is estimated to be 35% in the flux level and 0.2 in the power index.

The integral fluxes measured above 150 GeV lie in the range of 4% to 11% of the Crab Nebula flux measured by MAGIC (Albert et al. 2008a): the highest flux level is recorded in 2008 (0.11 Crab units³⁵), a factor between two to three larger compared to the one measured in 2007 (0.04 Crab units) and 2009 (0.05 Crab units). A constant fit to the data has a probability smaller than 0.001%. Such changes in the flux level observed in PG 1553+113 are quite moderate in comparison to other monitored TeV blazars. For example, in Mkn 421 flux variations exceeding one order of magnitude have been observed (e.g., Fossati et al. 2008).

A detailed study about possible flux level variations on short timescales was carried out with the limiting condition that the signal is not strong enough to allow for a detailed sampling on sub-day timescale. The upper panel of Figure 1 displays the light curve of PG 1553+113 measured from 2007 to 2009 by MAGIC with a variable binning. For comparison, the daily flux levels measured in 2005 and 2006 are shown, as extrapolated from the published data (Albert et al. 2007a), and rescaled according to the power laws that interpolate the differential fluxes. Furthermore, the 2006 mean integral flux above 150 GeV taken during the multiwavelength campaign and reported in Albert et al. (2009) is shown. The former data have not been used for the integral flux study, due to very large uncertainties related to the extrapolation procedure. We set 2 days, daily and monthly binning for the 2007, 2008, and 2009 data sets, respectively, according to the significance of the signal. The 2008 data are consistent with the hypothesis of constant flux with a probability of 50% (Figure 2, lower panel).

In 2007, the observed time series is consistent with constant flux (93% of probability). Nothing similar can be concluded for the 2009 observations since the significance of the signal is too low.

In general, the high energy threshold of the analysis together with the weakness of the PG 1553+113 signal and its very steep spectrum make any variability study at short timescale difficult and might have hidden the detection of an increased activity on very short timescale.

3.2. Differential Flux

The differential spectra observed from PG 1553+113 by MAGIC each year from 2007 to 2009 are shown in the left plot of Figure 3.

As for other blazars, each spectrum can be well fitted with a power-law function of the form

$$\frac{dF}{dE} = f_0 * \left(\frac{E}{200 \text{ GeV}} \right)^{-\Gamma}, \quad (1)$$

where f_0 is the flux at 200 GeV and Γ is the power-law index. The resulting indices are listed in the last column of Table 3. The systematic uncertainty is estimated to be 35% in the flux level and 0.2 in the power index (Albert et al. 2008a), and is the sum of many contributions, mainly related to the use of MC simulations instead of test beams. Thanks to the low energy threshold of the analysis of the 2007 data, the corresponding spectrum has a measured point below 100 GeV. In particular, the measured differential energy flux at 98 GeV is $(2.7 \pm 0.3) \times 10^{-9} \text{ cm}^{-2} \text{ s}^{-1} \text{ TeV}^{-1}$, in agreement, within the errors, with the low-energy point measured in 2005 and 2006, $(4.1 \pm 1.2) \times 10^{-9} \text{ cm}^{-2} \text{ s}^{-1} \text{ TeV}^{-1}$ at 97 GeV.

The 2008 differential energy spectrum measured above 150 GeV has a slope of 4.3 ± 0.4 , while the slope of the spectrum determined with a partially simultaneous sample taken during a multiwavelength campaign with other instruments is 3.4 ± 0.1 between 70 and 350 GeV (Aleksić et al. 2010). The different energy range characterizing the measurements fully accounts for this apparent disagreement: the spectral points measured in the range 150–350 GeV are, in fact, in very good agreement.

Finally, the 2009 differential spectrum is barely determined due to the limited signal. Except for the latter sample, whose significance is rather low and corresponding errors noticeably large, the power-law indices describing the spectra are compatible. This indicates that the shape of the emitted spectrum does not change, even if the total flux shows hints of (small amplitude) variability, as also noted for other BL Lac objects such as 1ES 1218+304 (Acciari et al. 2010).

The right plot of Figure 3 shows the combined differential spectrum of PG 1553+113 from 2007 to 2009, superimposed on the 2005–2006 spectrum measured by MAGIC ($\Gamma = 4.21 \pm 0.25$; Albert et al. 2007a). The gray band represents the systematic effect on the combined spectrum resulting from the use of different methods to correct for the effects due to the finite energy resolution (procedure called *unfolding*; Albert et al. 2007b). The good agreement among these mean determinations suggests that despite the (small) variability seen on yearly scale, the mean flux emitted by this source is stable. A power-law fit gives the values $\Gamma = 4.27 \pm 0.14$ for the index and $f_0 = (1.61 \pm 0.14) \times 10^{-10} \text{ s}^{-1} \text{ cm}^{-2} \text{ TeV}^{-1}$ for the normalization factor, with a $\chi^2/\text{dof} = 5.7/9$ and a corresponding probability of 77%. The integral flux above 150 GeV is at the level of 8% of the Crab Nebula flux.

³⁵ The Crab unit used in this work is an arbitrary unit obtained by dividing the integral energy flux measured above a certain threshold by the Crab Nebula flux measured above the same threshold by MAGIC (Albert et al. 2008a).

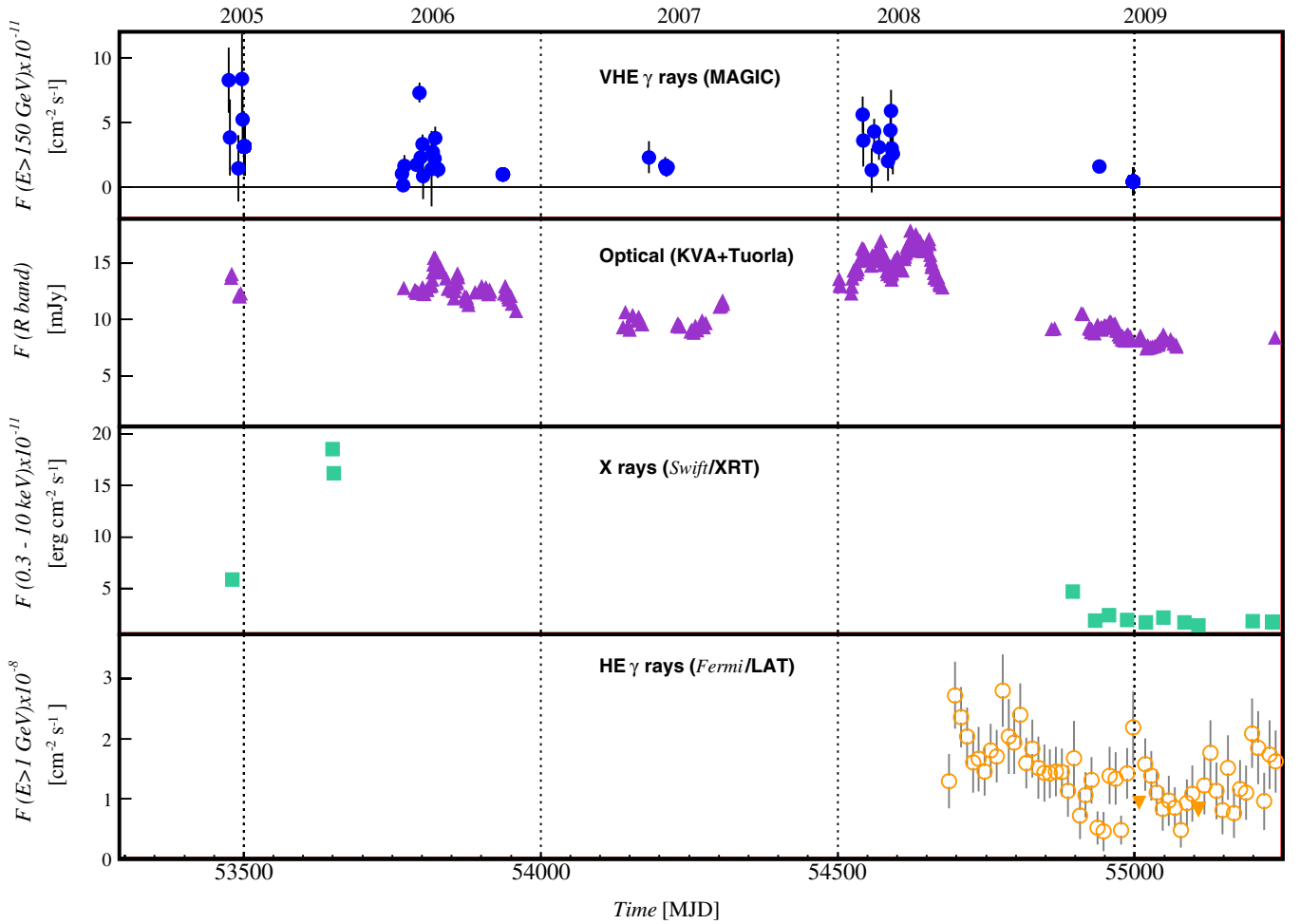


Figure 1. Multiwavelength light curve of PG 1553+113 from 2005 to late 2009. From upper to lower panel: VHE γ -rays above 150 GeV measured by MAGIC (filled circles), optical flux in the R band (triangles), X-rays 0.3–10 keV flux (squares), and γ -rays above 1 GeV (open circles). The error bars reported have 1σ significance. Downward triangles, in lower panel, refer to 2σ upper limits on the source flux above 1 GeV.

(A color version of this figure is available in the online journal.)

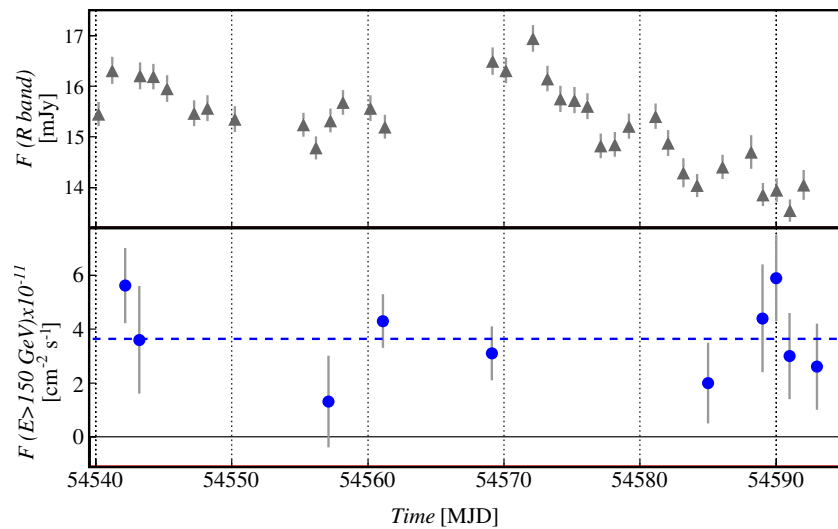


Figure 2. Zoom of Figure 1 around 2008 MAGIC observations (lower panel). In the upper panel the corresponding optical flux has been superimposed for comparison.

VHE photons from cosmological distances are absorbed in the interaction with the EBL. Taking into account the EBL absorption assuming the background model proposed in

Dominguez et al. (2011) and a redshift $z = 0.40$, the intrinsic spectrum is compatible with a power law of index 3.09 ± 0.20 , as drawn in Figure 3. If we assume $z = 0.45$, the

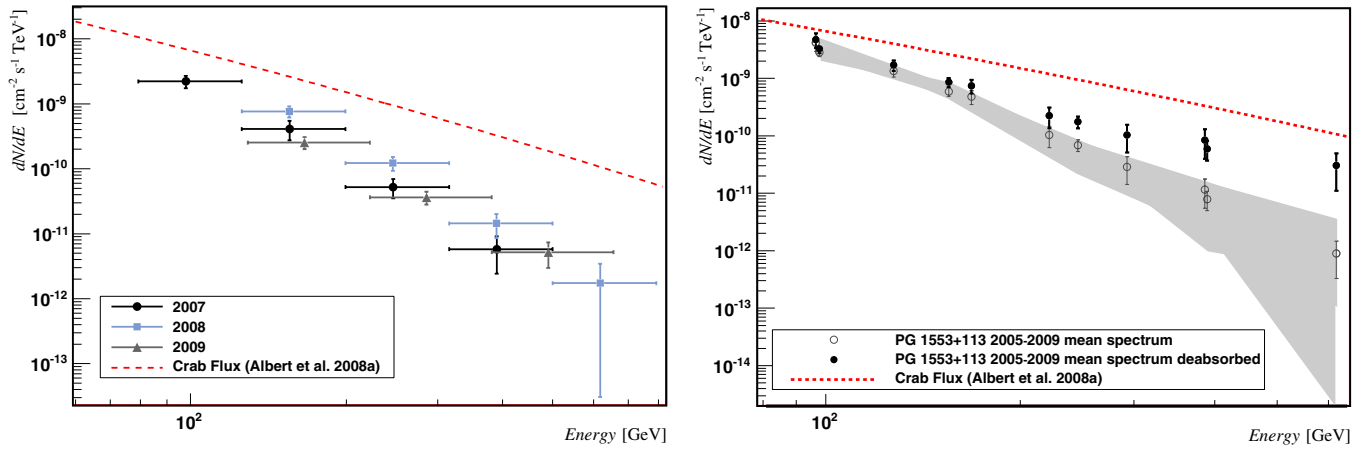


Figure 3. Differential energy spectra from PG 1553+113. Left: comparison between 2007, 2008, and 2009 spectra. Right: superimposition of 2005–2006 spectrum, from Albert et al. (2007a), to 2007–2009 mean spectrum and corresponding deabsorption for $z = 0.4$ using the EBL model of Dominguez et al. (2011). In both figures, the fit of the Crab Nebula spectrum measured by MAGIC (Albert et al. 2008a) is superimposed for comparison.

(A color version of this figure is available in the online journal.)

corresponding spectrum is compatible with a power law of index 2.91 ± 0.21 .

4. PG 1553+113 AS SEEN AT OTHER WAVELENGTHS

Figure 1 displays the light curve of PG 1553+113 in different wavelengths. The MAGIC data shown cover five cycles of TeV observations at energies above 150 GeV. The time bins used are variable, as described in the previous section.

The simultaneous optical R -band data are outlined in the second panel. These data are collected on a nightly basis by the Tuorla Observatory Blazar Monitoring Program³⁶ (Takalo et al. 2007) using the KVA 35 cm telescope at La Palma and the Tuorla 1 m telescope in Finland.

For the third panel in Figure 1 we used the 14 *Swift* pointed observations (Gehrels et al. 2004) of PG 1553 + 113 performed from 2005 April 20 to 2010 February 5. We summed the data collected on 2009 July 5 and 7 in order to have enough statistics to obtain a good spectral fit. The X-Ray Telescope (XRT) data were processed with standard procedures (xrtpipeline v0.12.6), filtering, and screening criteria by using the Heasoft package (v6.11). We consider the data collected in photon counting mode, and thus only XRT event grades 0–12 were selected.

Source events were extracted from a circular region with a radius of 20 pixels (1 pixel $\sim 2''.36$), while background events were extracted from a circular region with a radius of 50 pixels away from the source region. Some observations showed an average count rate of >0.5 counts s^{-1} , thus pile-up correction was required. In that case we extracted the source events from an annular region with an inner radius from 2 to 7 pixels (depending on the source count rate and estimated by means of the PSF fitting technique; see Moretti et al. 2005) and an outer radius of 30 pixels. We extracted background events within an annular region centered on the source with radii 70 and 120 pixels. Ancillary response files were generated with xrtmkarf and account for different extraction regions, vignetting and PSF corrections. We used the last spectral redistribution matrices in the Calibration database maintained by HEASARC. All spectra were rebinned with a minimum of 20 counts per energy bin to allow χ^2 fitting within XSPEC (v12.7.0; Arnaud 1996). We

fit the spectrum with an absorbed (model *tbabs* in Xspec) log parabola law (see, e.g., Tramacere et al. 2007), with a neutral hydrogen column fixed to its Galactic value (3.65×10^{20} cm^{-2} ; Kalberla et al. 2005). The observed 0.3–10 keV fluxes obtained by *Swift*/XRT in the different observations are reported in the third panel of Figure 1.

In the lower panel, the *Fermi*/LAT light curve of PG 1553+113, computed in 10 day bins, is displayed. *Fermi* data presented in this paper are restricted to the 1 GeV–100 GeV energy range and were collected from MJD 54682 (2008 August 4) to MJD 55200 (2010 January 4) in survey mode.

An unbinned analysis was performed to produce the light curve with the standard analysis tool *gtlike*, included in the Science Tools software package (version v09r21p00). P6_V11 DIFFUSE Instrument Response Functions (IRFs) were used, which are a refinement to previous analyses reflecting improved understanding of the PSF and effective area (A. A. Abdo et al. 2012, in preparation). For this analysis, only photons belonging to the Diffuse class and located in a circular region of interest (ROI) of 10° radius, centered at the position of PG 1553+113, were selected. In addition, we excluded photons arriving from zenith angles $>105^\circ$ to limit contamination from Earth limb γ -rays and photons with rocking angles $>52^\circ$ to avoid time intervals during which Earth entered the LAT FoV.

A separate analysis of the high-energy emission in each time bin was performed. All point sources in the 1FGL within 15° of PG 1553+113, including the source of interest itself, were considered in the analysis. Those within the 10° radius ROI were fitted with a power law with spectral indices frozen to the values obtained from the likelihood analysis of the full data set, while those beyond 10° radius ROI had their values frozen to those found in 1FGL.

Upper limits at 2σ confidence level (downward triangles in Figures 1 and 4) were computed for time bins with Test Statistics (TS)³⁷ < 4 and were handled as in the first *Fermi*/LAT catalog paper. The estimated systematic uncertainty on the flux is 10% at 100 MeV, 5% at 500 MeV, and 20% at 10 GeV.

As already noted, during the five years of monitoring the source generally showed a marginal activity in the VHE γ -ray band. The same behavior is followed by the optical flux, whose

³⁶ More information at <http://users.utu.fi/kani/1m/>

³⁷ TS is two times the difference of the log(likelihood) with and without the source (Mattox et al. 1996).

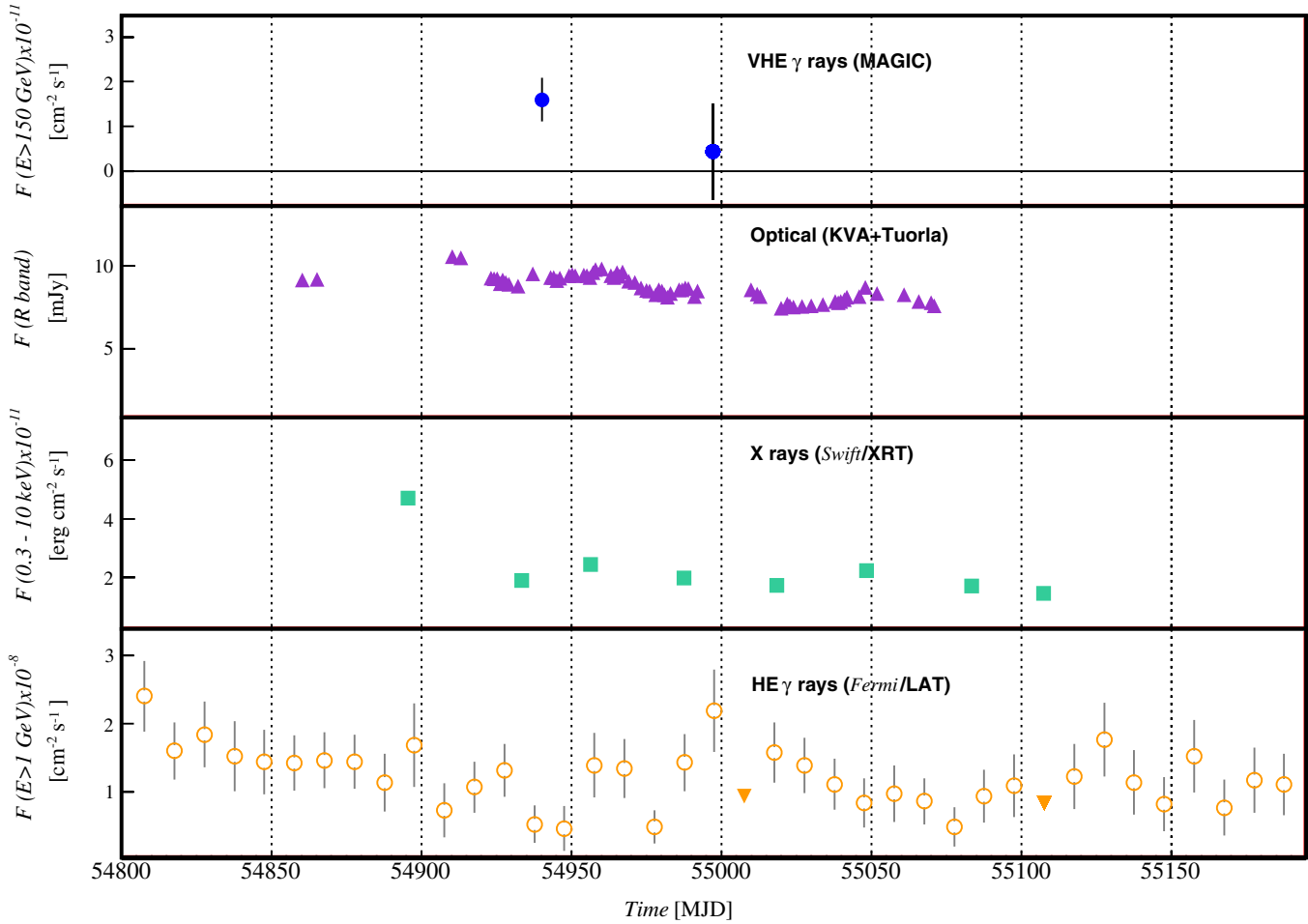


Figure 4. Zoom of Figure 1 around the Cycle V observations carried out in 2009. From upper to lower panel: VHE γ -rays above 150 GeV measured by MAGIC (filled circles), optical flux in the R band (triangles), X-rays 0.3–10 keV flux (squares), and soft γ -rays above 1 GeV (open circles). Downward triangles, in lower panel, refer to 2σ upper limits on the source flux above 1 GeV.

(A color version of this figure is available in the online journal.)

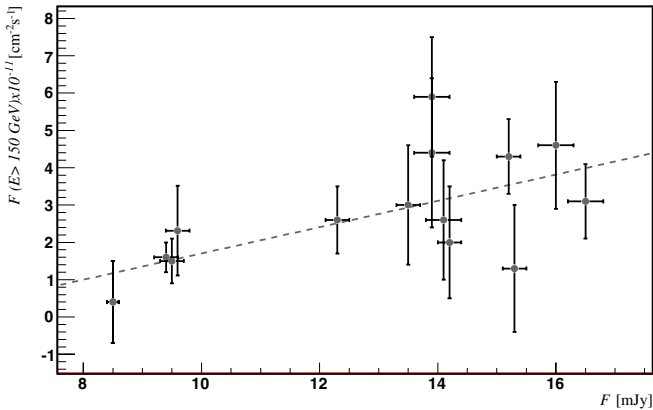


Figure 5. Correlation study between PG 1553+113 optical R -band flux and VHE γ -ray integral flux above 150 GeV observed from 2006 to 2009.

variations are limited within a factor of four, with a maximum flux reached in 2008 and a minimum value in 2009. A low emission in 2009 is also registered at all the other wavelengths, Figure 4, suggesting that the source entered in a low-activity state during that year, with a minimum reached few days after MAGIC observations.

Figure 5 shows the result of a correlation study between optical and TeV simultaneous observations. The VHE γ -ray

flux above 150 GeV is plotted as a function of the optical flux. In order to increase statistics, we used for 2007 August 9 samples the daily light curve values; however, since the optical measurements have a different time coverage, in some cases we derived the mean VHE flux from two or more consecutive days. 2005 and 2006 data from Albert et al. (2007a) were rejected from this study, due to the large uncertainty on the extrapolated flux in the VHE band. The mean flux value from 2006 multiwavelength campaign, reported in Albert et al. (2009), is included. A linear relation among the two components has a 74% probability, which suggests a correlation between these two extreme energy bands. This result is in good agreement with the SSC model, which predicts a correlation between the synchrotron and the IC emission, related to the same electron population. Due to the poor simultaneity of VHE data with the other wavelengths, the same study has not been performed in X-rays and soft γ -rays.

The X-ray light curve shows a pronounced variability, in contrast to optical and VHE bands. The X-ray flux spans an interval of about one order of magnitude (with maximum in 2005 and minimum in 2009), larger than that observed in the TeV, optical, and GeV bands. The different variability displayed by the synchrotron (X-ray) and inverse Compton (GeV–TeV) components seems to be somewhat in contrast with the typical behavior observed in TeV BL Lac objects, showing, in general,

a coordinated variability (e.g., Fossati et al. 2008).³⁸ However, the sparse sampling of the observations and the lack of a truly simultaneous monitoring prevents any strong conclusion. In particular, no optical nor gamma-ray data are available during the period of the maximum X-ray flux in 2005. Coordinated multifrequency monitoring is necessary to further investigate this important issue.

In a dedicated paper (Abdo et al. 2010b), the *Fermi*/LAT collaboration reported the analysis of the first year of PG 1553+113 data. They found that during the monitoring period the emission above 200 MeV is almost steady. This is in contrast with the behavior of the source at higher energies (> 1 GeV). In our analysis of 2008 and 2009 LAT data (drawn in lower panel of Figure 1), in fact, a steady emission above 1 GeV has a probability smaller than 0.1% and is ruled out. The lowest flux, observed in 2009 April, has a value of $(0.5 \pm 0.3) \times 10^{-8} \text{ cm}^{-2} \text{ s}^{-1}$, while the highest flux, detected in 2008 August, has a value of $(2.8 \pm 0.6) \times 10^{-8} \text{ cm}^{-2} \text{ s}^{-1}$, more than five times higher. In our case, we are looking only at the upper edge of the LAT band, probably close to the IC peak, while the integral flux above 200 MeV reported by Abdo et al. (2010b) is dominated by lower energies due to larger statistics. Therefore, we conclude that while at low energies (200 MeV–1 GeV) the IC continuum shows only marginal variability, this is not the case in the vicinity of the peak (some GeVs). In fact, small variability at GeV energies is a common feature of HBLs (Abdo et al. 2010a).

5. MODELING THE SED

In Figure 6, we assembled the SED of PG 1553+113 using historical data and the MAGIC spectra described above. Open black squares displaying radio-optical data are from NED.³⁹ In the optical band, we also show (red diamonds) the KVA minimum and maximum fluxes measured in the period covered by MAGIC 2005–2009 observations together with optical–UV fluxes from *Swift*/UVOT (filled black triangles from Tavecchio et al. 2010). For the X-ray data, two *Swift*/XRT spectra taken in 2005 (high-flux state, red crosses, and intermediate state, black asterisks, from Tavecchio et al. 2010) are given, and a *Suzaku* spectrum taken in 2006 (continuous red line from Reimer et al. 2008). In addition, the average 15–150 keV flux measured by *Swift*/BAT during the first 54 months of survey (Cusumano et al. 2010) is shown (black star), and the average *RXTE*/ASM flux between 2008 March 1 and May 31 (small black square), from quick-look results provided by the *RXTE*/ASM team.⁴⁰

The green triangles correspond to the LAT spectrum averaged over ~ 200 days (2008 August–2009 February) from Abdo et al. (2010b). As discussed in that paper, the flux above 200 MeV is rather stable, showing very small variability over the entire period of LAT observations. It is likely that the variability observed at the highest energies is not important in determining the averaged spectrum due to the limited statistics.

For MAGIC, we report the 2005–2006 and 2007–2009 observed spectra (filled circles) and the same spectra corrected for the absorption by the EBL using the model of Dominguez et al. (2011; red open circles).

We model the SED with the one-zone SSC model fully described in Maraschi & Tavecchio (2003). The emission zone is supposed to be spherical with radius R , in motion with bulk

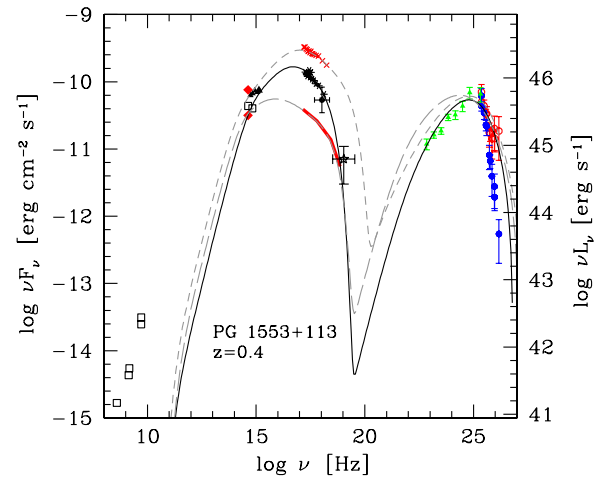


Figure 6. SED of PG 1553+113. Open black squares represent the radio-optical data from NED, red diamonds represent the KVA minimum and maximum fluxes measured in the period covered by MAGIC observations, together with optical–UV fluxes from *Swift*/UVOT (filled black triangles). For the X-ray data, two *Swift*/XRT spectra taken in 2005 (high-flux state, red crosses, and intermediate state, black asterisks) are given, and a *Suzaku* spectrum taken in 2006 (continuous red line). The average 15–150 keV flux measured by *Swift*/BAT (black star) and the average *RXTE*/ASM flux between 2008 March 1 and May 31 (small black square) are also represented. The LAT spectrum averaged over ~ 200 days (2008 August–2009 February) is given (green filled triangles). For MAGIC, we display the 2005–2006 and 2007–2009 observed spectra (blue filled circles) and the same spectra corrected for the absorption by the EBL (red open circles). The average SED is modeled with a one-zone SSC model (continuous black line). Alternative SEDs are superimposed in light gray. Detailed references are addressed in the text.

(A color version of this figure is available in the online journal.)

Lorentz factor Γ at an angle θ with respect to the line of sight. Special relativistic effects are described by the relativistic Doppler factor, $\delta = [\Gamma(1 - \beta \cos \theta)]^{-1}$. The energy distribution of the relativistic emitting electrons is described by a smoothed broken power-law function, with limits γ_{\min} and γ_{\max} and break at γ_b . To calculate the SSC emission, we use the full Klein–Nishina cross section.

Given the large variations of the X-ray synchrotron flux, we decided to use the average level of the synchrotron bump as measured by XRT, including also ASM and BAT fluxes to constrain the model. The corresponding input parameters are listed in Table 4. We also report the derived powers carried by the different components, relativistic electrons, P_e , magnetic field, P_B , and protons, P_p (assuming a composition of one cold proton per relativistic electron) and the total radiative luminosity $L_r \simeq L_{\text{obs}}/\delta^2$.

In order to investigate the role of different parameters in the model, we have explored their variation as a function of the intensity of the synchrotron peak. To do so, we have modeled the SED considering the two extreme states of the synchrotron peak described above, respectively. For the SSC peak, instead, we have fixed the VHE data. The two curves representing the models are superimposed in light gray on Figure 6. The parameters obtained, listed in the last two columns of Table 4, are quite similar to the ones obtained when considering the average level of the synchrotron bump, except for the two variables B and K, the magnetic field, and the electron density. Indeed, these two parameters regulate the relative importance of synchrotron and SSC components. The state characterized by a low-synchrotron emission has larger B and smaller K values with respect to the mean state modeled above. Conversely, the high-synchrotron emission state has smaller values of B and a larger K.

³⁸ Rare exceptions to this rule are the so-called orphan TeV flares, e.g., Krawczynski et al. (2004).

³⁹ <http://nedwww.ipac.caltech.edu/>

⁴⁰ <http://xte.mit.edu/asmlc/>

Table 4
Input Model Parameters for the Models Shown in Figure 6

Parameter	Units	Value _{mean}	Value _{max}	Value _{min}
γ_{\min}	[10^3]	2.5	1	5
γ_b	[10^4]	3.2	3	1.3
γ_{\max}	[10^5]	2.2	5.2	4.1
n_1		2.0	2.0	2.0
n_2		4.0	3.75	3.55
B	[G]	0.5	0.8	0.2
K	[10^3 cm^{-3}]	5.35	3.8	25
R	[10^{16} cm]	1	1	1
δ		35	35	35
P_e	[$10^{44} \text{ erg s}^{-1}$]	2.2		
P_B	[$10^{44} \text{ erg s}^{-1}$]	1.5		
P_p	[$10^{44} \text{ erg s}^{-1}$]	0.34		
L_r	[$10^{44} \text{ erg s}^{-1}$]	6.3		

Notes. We list for the three different models plotted in Figure 6 the minimum, break and maximum Lorentz factors and the low- and high-energy slopes of the electron energy distribution, the magnetic field intensity, the electron density, the radius of the emitting region, and its Doppler factor. For the average model we also give the derived power carried by electrons, magnetic field, protons (assuming one cold proton per emitting relativistic electron), and the total radiative luminosity.

Finally, a comparison with the SED model obtained in the multiwavelength campaign reported in Aleksić et al. (2010) reveals that the parameters used for building the two models are quite similar. The major differences are the value of the Doppler factor, which in our model is relatively higher ($\delta = 35$) than in the previous one ($\delta = 23$), and that of the magnetic field (0.5 G instead of 0.7 G). This difference is mainly due to the higher SSC peak frequency that we find in our data, better defined by the combined LAT and MAGIC spectra.

The derived value of the total jet power, $P_{\text{jet}} = P_e + P_B + P_p = 4 \times 10^{44} \text{ erg s}^{-1}$, is consistent with the typical values inferred modeling similar sources (e.g., Ghisellini et al. 2011). We use a relatively large minimum electron Lorentz factor $\gamma_{\min} \sim 10^3$ in order to reproduce the hard MeV–GeV continuum tracked by LAT (photon index $\Gamma = 1.68 \pm 0.03$). The high value of γ_{\min} implies that, as commonly derived in TeV BL Lac objects, the relativistic electrons (and the magnetic field, almost in equipartition) carry more power than the cold proton component. Another characteristic that PG 1553+113 shares with the other TeV BL Lac objects is that the total luminosity L_r is larger than the power supplied by electrons, magnetic field, and protons. As discussed in Celotti & Ghisellini (2008), this implies that either only a small fraction of leptons is accelerated at relativistic energies (leaving a reservoir of cold pairs and/or protons) or that the jet is dissipating a large fraction of its power as radiation, eventually leading to the deceleration of the flow, as in fact observed at VLBI scales (Piner et al. 2010) and envisaged in the models of structured jets (Georganopoulos & Kazanas 2003; Ghisellini et al. 2005).

6. CONCLUSIONS

In this paper, we presented the analysis of three years of VHE γ -ray data of PG 1553+113 collected by MAGIC from 2007 to 2009. The data set was divided into individual years and a significant signal was found in every sample, confirming PG 1553+113 as a stable presence in the VHE sky. The overall flux above 150 GeV from 2007 to 2009 shows only a modest variability on a yearly timescale, within a factor three,

corresponding to a variation between 4% and 11% of the Crab Nebula flux. No clear variability on smaller time scales is evident in the sample.

For the spectral analysis, the data set was combined with previous observations carried out by MAGIC during the first two Cycles of operations, from 2005 to 2006, for a total of five years of monitoring. This sample was excluded from the temporal study due to very large systematics related to the flux extrapolation procedure. Despite the hints of variability on the flux level, the differential flux from each year is in very good agreement with a power law of constant index 4.27 ± 0.14 . This behavior has been already observed in other blazars, such as the HBL 1ES 1218+304 (Acciari et al. 2010).

PG 1553+113 was also monitored in optical, X-ray, and soft γ -ray frequencies, but only the former data could be used for correlation studies thanks to the large timing coverage. Interestingly, a hint of correlation with a probability of 74% was found between MAGIC and R-band optical flux levels, which in turn shows only a modest variability within a factor four. A clear variability is seen in the X-rays and γ -rays above 1 GeV. The latter outcome, exploring the energies close to the IC peak, is only apparently in contradiction with previous results stating a quite stable spectrum for this source in the soft ($>200 \text{ MeV}$) γ -ray band (Abdo et al. 2010b). The different energy thresholds used in the two studies can, in fact, explain very well the discrepancy, as discussed in this paper.

Finally, for the study of the SED, the mean differential spectrum measured by MAGIC was combined with historical data at other wavelengths. Due to the large variations observed in X-rays and characterizing the synchrotron peak, we decided to use for the SED modeling the high-energy bump and the average level of the low-energy bump. A more precise model requires coupling the VHE γ -ray part of the spectrum with simultaneous coverage of the synchrotron peak, in particular at optical–X-ray energies. An interesting feature of PG 1553+113 is the narrowness of the SSC peak derived from the LAT and MAGIC spectra, implying a relatively large value of the minimum Lorentz factor of the emitting electrons, 2.5×10^3 . This is also required by other HBLs with hard GeV spectra (e.g., Tavecchio et al. 2010).

The MAGIC stereo system, with its increased sensitivity and low energy threshold, is the suitable instrument to further investigate eventual daily scale TeV variability, as well as to provide a good differential spectrum determination below 100 GeV.

We thank the Instituto de Astrofísica de Canarias for the excellent working conditions at the Observatorio del Roque de los Muchachos in La Palma. The support of the German BMBF and MPG, the Italian INFN, the Swiss National Fund SNF, and the Spanish MICINN is gratefully acknowledged. This work was also supported by the Marie Curie program, by the CPAN CSD2007-00042 and MultiDark CSD2009-00064 projects of the Spanish Consolider-Ingenio 2010 programme, by the grant DO02-353 of the Bulgarian NSF, by the grant 127740 of the Academy of Finland, by the YIP of the Helmholtz Gemeinschaft, by the DFG Cluster of Excellence “Origin and Structure of the Universe,” by the DFG Collaborative Research Centers SFB823/C4 and SFB876/C3, and by the Polish MNiSzW grant 745/N-HESS-MAGIC/2010/0.

The *Fermi* LAT Collaboration acknowledges generous ongoing support from a number of agencies and institutes that have

supported both the development and the operation of the LAT as well as scientific data analysis. These include the National Aeronautics and Space Administration and the Department of Energy in the United States, the Commissariat à l'Énergie Atomique and the Centre National de la Recherche Scientifique/Institut National de Physique Nucléaire et de Physique des Particules in France, the Agenzia Spaziale Italiana and the Istituto Nazionale di Fisica Nucleare in Italy, the Ministry of Education, Culture, Sports, Science and Technology (MEXT), High Energy Accelerator Research Organization (KEK) and Japan Aerospace Exploration Agency (JAXA) in Japan, and the K. A. Wallenberg Foundation, the Swedish Research Council and the Swedish National Space Board in Sweden.

Additional support for science analysis during the operations phase is gratefully acknowledged from the Istituto Nazionale di Astrofisica in Italy and the Centre National d'Études Spatiales in France.

REFERENCES

- Abdo, A. A., Ackermann, M., Ajello, M., et al. 2009, *ApJ*, **700**, 597
- Abdo, A. A., Ackermann, M., Ajello, M., et al. 2010a, *ApJ*, **722**, 520
- Abdo, A. A., Ackermann, M., Ajello, M., et al. 2010b, *ApJ*, **708**, 1310
- Acciari, V. A., Aliu, E., Beilicke, M., et al. 2010, *ApJ*, **709**, L163
- Aharonian, F., Akhperjanian, A. G., Bazer-Bachi, A. R., et al. 2006a, *A&A*, **448**, L19
- Aharonian, F., Akhperjanian, A. G., Bazer-Bachi, A. R., et al. 2006b, *Nature*, **440**, 1018
- Albert, J., Aliu, E., Anderhub, H., et al. 2007a, *ApJ*, **654**, L119
- Albert, J., Aliu, E., Anderhub, H., et al. 2007b, *Nucl. Instrum. Methods Phys. Res. A*, **583**, 494
- Albert, J., Aliu, E., Anderhub, H., et al. 2008a, *ApJ*, **674**, 1037
- Albert, J., Aliu, E., Anderhub, H., et al. 2008b, *ApJ*, **685**, L23
- Albert, J., Aliu, E., Anderhub, H., et al. 2008c, *Nucl. Instrum. Methods Phys. Res. A*, **588**, 424
- Albert, J., Aliu, E., Anderhub, H., et al. 2009, *A&A*, **493**, 467
- Aleksić, J., Anderhub, H., Antonelli, L. A., et al. 2010, *A&A*, **515**, A76
- Aliu, E., Anderhub, H., Antonelli, L. A., et al. 2009, *Astropart. Phys.*, **30**, 293
- Arnaud, K. A. 1996, in ASP Conf. Ser. 101, *Astronomical Data Analysis Software and Systems V*, ed. G. H. Jacoby & J. Barnes (San Francisco, CA: ASP), 17
- Baixaeras, C., Bastieri, D., Bigongiari, C., et al. 2004, *Nucl. Instrum. Methods Phys. Res. A*, **518**, 188
- Britzger, D., Carmona, E., Majumdar, P., et al. 2009, in Proc. 31st Int. Cosmic Ray Conf., preprint (arXiv:0907.0973)
- Celotti, A., & Ghisellini, G. 2008, *MNRAS*, **385**, 283
- Cortina, J., Goebel, F., & Schweizer, T. 2009, arXiv:0907.1211
- Cusumano, G., La Parola, V., Segreto, A., et al. 2010, *A&A*, **524**, A64
- Danforth, C. W., Keeney, A. B., Stocke, J. T., Michael Shull, J., & Yao, J. 2010, *ApJ*, **720**, 976
- Dominguez, A., Primack, J. R., Rosario, D. J., et al. 2011, *MNRAS*, **410**, 2556
- Fomin, V. P., Stepanian, A., Lamb, R. C., et al. 1994, *Astropart. Phys.*, **2**, 137
- Fossati, G., Buckley, J. H., Bond, I. H., et al. 2008, *ApJ*, **677**, 906
- Gehrels, N., Chincarini, G., Giommi, P., et al. 2004, *ApJ*, **611**, 1005
- Georganopoulos, M., & Kazanas, D. 2003, *ApJ*, **594**, L27
- Ghisellini, G., Tavecchio, F., & Chiaberge, M. 2005, *A&A*, **432**, 401
- Ghisellini, G., Tavecchio, F., Foschini, L., & Ghirlanda, G. 2011, *MNRAS*, **414**, 2674
- Green, R. F., Schmidt, M., & Liebert, J. 1986, *ApJS*, **61**, 305
- Kalberla, P. M. W., Burton, W. B., Hartmann, D., et al. 2005, *A&A*, **440**, 750
- Krawczynski, H., Hughes, S. B., Horan, D., et al. 2004, *ApJ*, **601**, 151
- Li, T. P., & Ma, Y. Q. 1983, *ApJ*, **272**, 317
- Mannheim, K. 1993, *A&A*, **269**, 67
- Maraschi, L., & Tavecchio, F. 2003, *ApJ*, **593**, 667
- Mattox, J. R., Bertsch, D. L., Chiang, J., et al. 1996, *ApJ*, **461**, 396
- Mazin, D., & Goebel, F. 2007, *ApJ*, **655**, L13
- Moretti, A., Campana, S., Mineo, T., et al. 2005, Proc. SPIE, **5898**, 360
- Piner, B. G., Pant, N., & Edwards, P. G. 2010, *ApJ*, **723**, 1150
- Prandini, E., Bonnoli, G., Maraschi, L., Mariotti, M., & Tavecchio, F. 2010, *MNRAS*, **405**, L76
- Reimer, A., Costamante, L., Madejski, G., Reimer, O., & Dorner, D. 2008, *ApJ*, **682**, 775
- Sbarufatti, B., Treves, A., & Falomo, R. 2005, *ApJ*, **635**, 173
- Sbarufatti, B., Treves, A., Falomo, R., et al. 2006, *AJ*, **132**, 1
- Stecker, F. W., de Jager, O. C., & Salamon, M. H. 1992, *ApJ*, **390**, L49
- Takalo, L. O., Nilsson, K., Lindfors, E., Pasanen, M., & Berdyugin, A. 2007, in ASP Conf. Ser. 373, *The Central Engine of Active Galactic Nuclei*, ed. L. C. Ho & J.-M. Wang (San Francisco, CA: ASP), 249
- Tavecchio, F., Ghisellini, G., Ghirlanda, G., Foschini, L., & Maraschi, L. 2010, *MNRAS*, **401**, 1570
- Tramacere, A., Massaro, F., & Cavaliere, A. 2007, *A&A*, **466**, 521
- Urry, C. M., & Padovani, P. 1995, *PASP*, **107**, 803